Electronic Supplementary Material (ESI) for Sensors & Diagnostics.

Flexible & Transparent Breath Sensor and Conducting Electrodes Based on Highly Interconnected Au Nanoparticle Network

Namuni Sneha and S. Kiruthika*

Dr. S. Kiruthika, Namuni Sneha

Department of Physics, School of Electrical and Electronics Engineering,

SASTRA Deemed to be University, Thanjavur 613 401, Tamil Nadu, India

Email: kiruthika@ece.sastra.edu

Figure S1

XPS core level spectra:

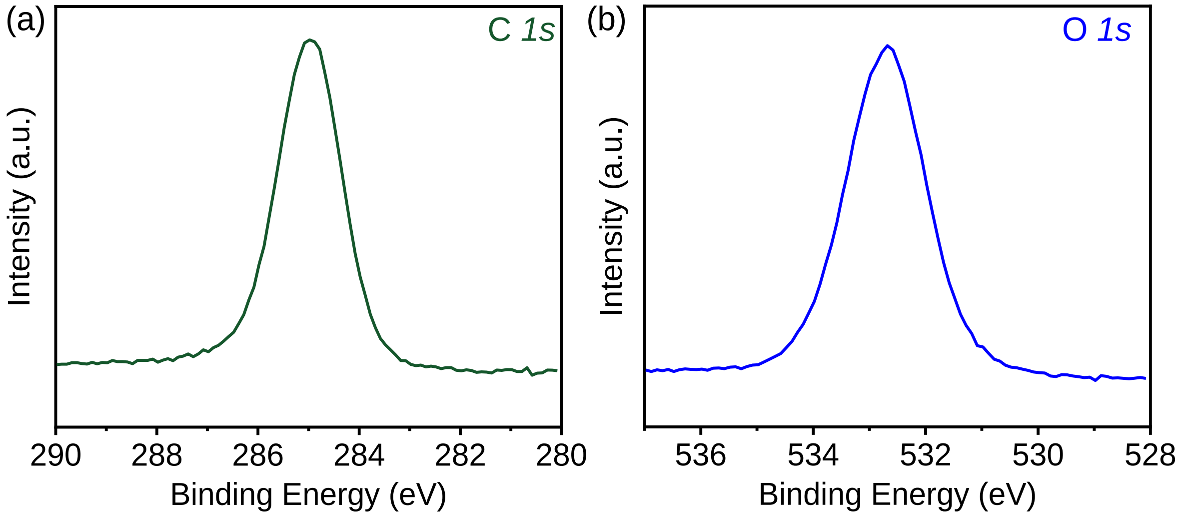

Fig. S1. X-ray photoelectron spectroscopy core level spectra of (a) C *1s* and (b) O *1s* of Au-1L nanonetwork on the glass substrate.

Fig. S1a represents the high-resolution core-level spectrum of carbon (C *1s*), showing its binding energy peak at 284.98 eV and the oxygen (O *1s*) peak appeared at 532.68 eV (**Fig. S1b**).

Figure S2

XRD of as-prepared Au nanonetwork:

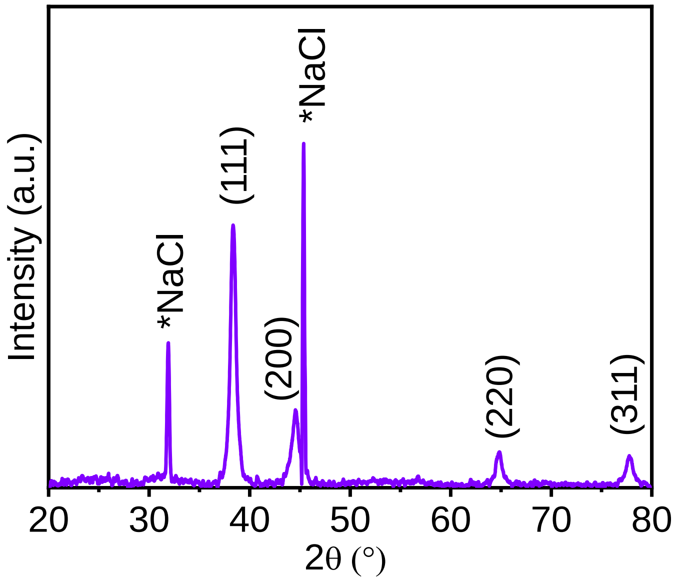

Fig. S2. XRD pattern of as-prepared gold nanonetwork (Au-5L) on a glass substrate.

Fig. S2 shows the X-ray diffraction pattern of the as-prepared Au-5L network, showing the peaks of both crystalline Au and sodium chloride (NaCl). To remove the NaCl crystals, the TCEs were gently rinsed in DI water and dried in air. The XRD of the washed TCEs clearly showed the absence of any NaCl peaks (**Fig. 2i**)

Figure S3

Transmittance spectra and I-V characteristics of Au TCE:

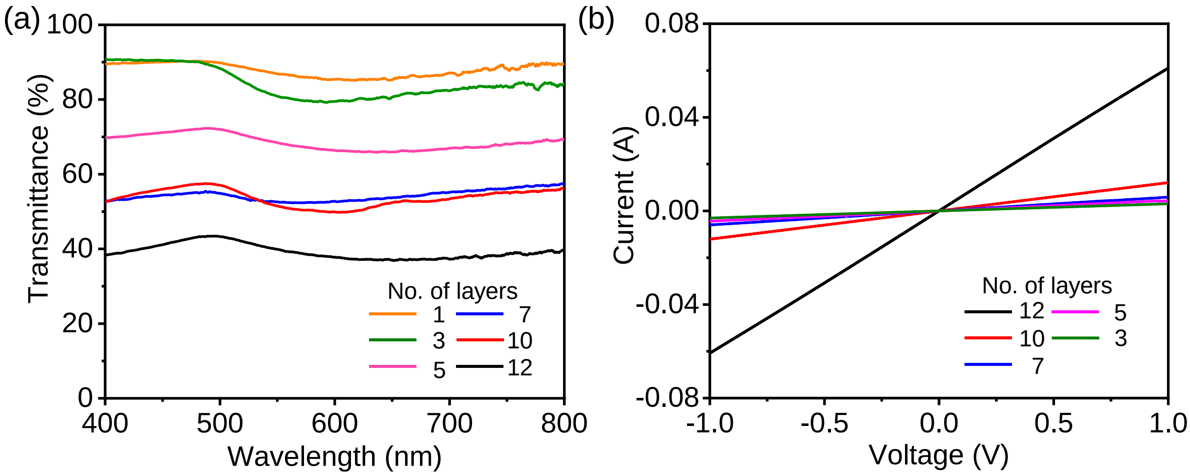

Fig. S3 (a) Transmittance spectra (400-800 nm) and (b) I-V characteristics of different Au nanonetwork layers ranging from 1-12.

Figure S4

Photographs of Au TCEs:

Fig. S4 Photographs of Au-1L, 5L, 12L nanonetworks (glass substrates)

Figure S5

Au nanonetwork/PDMS:

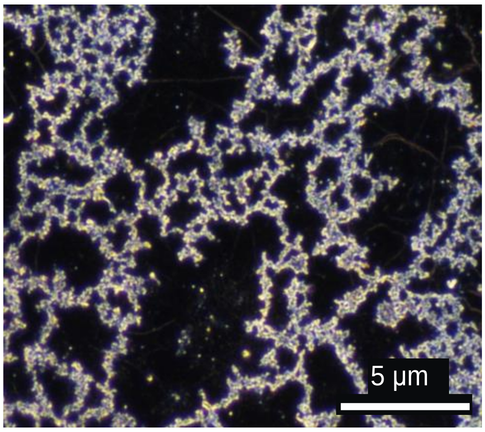

Fig. S5 Optical microscope image of interconnected Au nanonetwork (Au-12L) transferred over flexible PDMS substrate.

Figure S6

Scotch tape test:

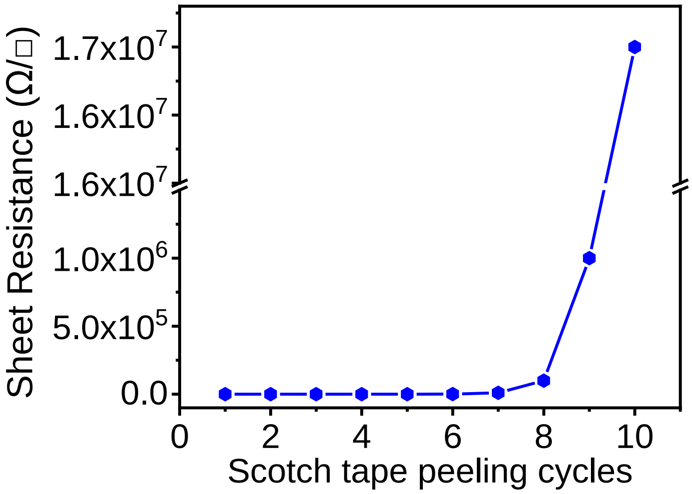

Fig. S6 Change in sheet resistance of Au-12L nanonetwork during scotch tape adhesion test.

Figure S7

Transmittance of Au-1L device:

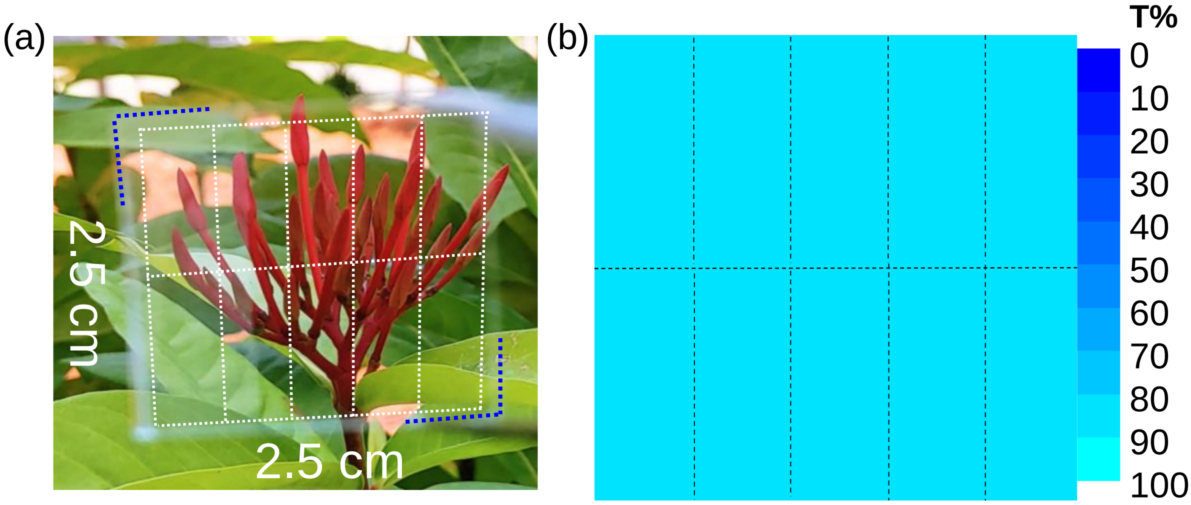

Fig. S7 (a) The photograph of the Au-1L nanonetwork. The grid pattern drawn over the photo indicates the specific pixel region utilized for transmittance measurements shown in Fig. S7b. (b) The contour plot depicting the uniformity in transmittance (at 550 nm) of the Au-1L nanonetwork across 2.5 × 2.5 cm^2.

The transmittance was measured across the different locations on the device to study the uniformity of the Au nanonetwork over the substrate. The photograph of the highly transparent Au-1L nanonetwork (2.5 × 2.5 cm^2) is shown in **Fig. S7a**. The transmittance at 550 nm is represented as the contour plot in **Fig. S7b**. From the contour plot, it is inferred that the Au-1L nanonetworks exhibit consistent transmittance of >80% across different regions. The white grid pattern drawn over the photo of Au-1L in **Fig. S7a** indicates the specific pixel region utilized for transmittance measurements.

<u>Figure S8</u>

<u>Transmittance plots Au-1L device:</u>

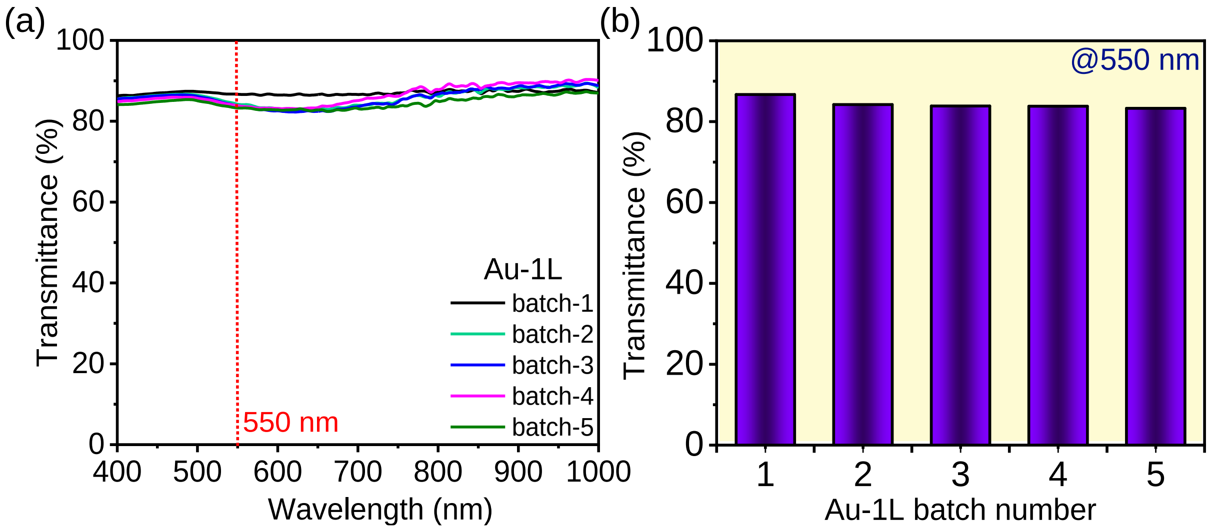

Fig. S8 (a) Transmittance spectra of Au-1L nanonetwork in the 400-1000 nm range, prepared during five different batches in the consecutive synthesis cycles under similar experimental conditions and comparing its transmittance at 550 nm (b).

Fig.S8 represents the optical transmittance of Au-1L nanonetworks fabricated in 5 different batches (glass substrates), exhibiting a high transmittance (> 80%) between 400 to 1000 nm. The standard deviations of T% (at 550 nm) for all five samples are 84.34 ± 1.35%.

<u>**Figure S9**</u>

<u>**I-V characteristics of Au-1L device:**</u>

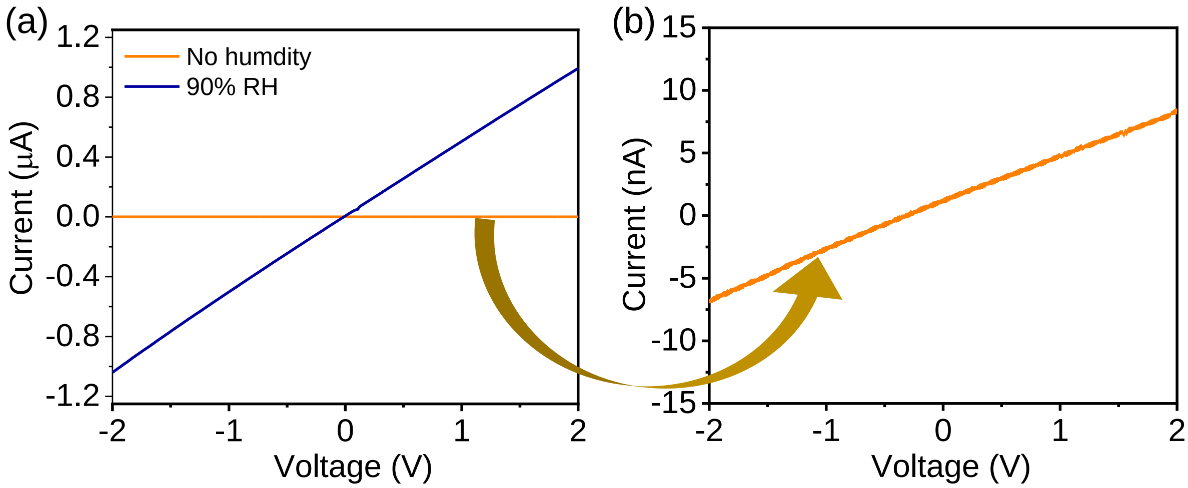

Fig. S9 (a) Comparing the I-V characteristics of Au-1L nanonetwork-based sensor in the presence and absence of humidity. (b) I-V characteristics of Au-1L sensor.

Figure S10

Humidity sensing of Au-1L device:

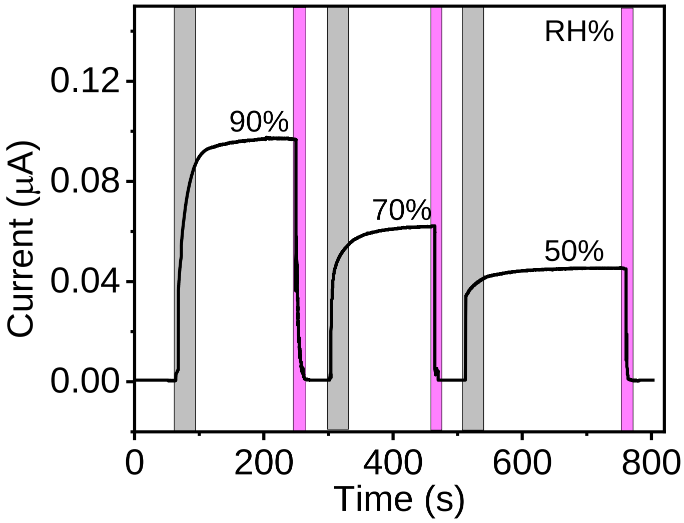

Fig. S10 Variation in response current of Au-1L breath sensor at different relative humidities (RH%)

<u>Figure S11</u>

<u>Detecting breathing and blowing air using the Au-1L sensor:</u>

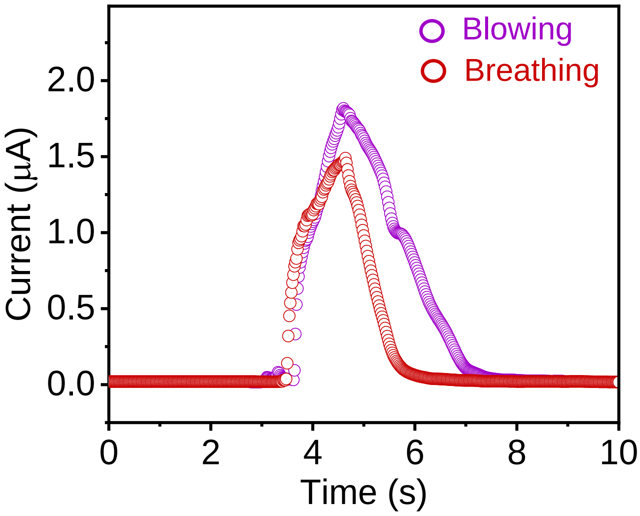

Fig. S11 The Au-1L sensor detects a volunteer's response while breathing out through the nose (breathing) and mouth (blowing) at a 1 cm working distance.

Fig. S11 shows that the current variation of the sensor during the mouth blowing is slightly larger than that of the nose breathing, revealing that more water molecules are captured while blowing.

Table S1. Comparing the main characteristics of humidity/human breath sensor developed in this study with recent literatures.

Substrate	Sensing material	Fabrication method	Transmit-tance (%)	Flex-ibility	Stretch-ability	Thermal stability	Aging effect	Output signal for sensor	[a]Response/[b]Recovery time (s)	Ref.
Glass/ FTO	MoO_{3-x}	Liquid-phase exfoliated	>80%	NO	NO	-	-	Current	a = 0.12 b = 0.53	1
PEN/ITO	Graphene oxide	Modified Hummer's method and electrostatic spray deposition technique	>60%	YES	NO	tested up to 80 °C	-	Impedance	a = 5 b = 11	2
Cellulose	Cellulose/KOH composite ionic film	Water-evaporation-induce dense packing	87.14% @550 nm	YES	YES	tested up to 240 °C	tested up to 5 weeks	Resistance	a = 6.0 b = 10.8 @97.3 RH%	3
PDMS	Graphene /WS_2 thin film	Metal sulfurization and reactive ion etching.	>70%	YES	YES	-	stable up to several months	Current	a = 5 b = 6	4
Nanocellulose	TiO_2/cellulose nanocrystal	Enzymatic method and electrostatic self-assembly process	84.5% (600 nm)	YES	YES	stable up to 346 °C	>40 days	Resistance	a=22 b=13 @95% RH	5
PET	Gallium-doped ZnO and poly-methyl methacrylate (PMMA) and [3-(methacrylamino)propyl] trimethyl ammonium chloride	RF magnetron sputtering and brush-coating	>70% (400-700 nm)	YES	NO	-	55 days	Impedance	a = 70 b = 90	6
PET	ITO	Magnetron sputtering	75-82% (380-800 nm)	YES	NO	-	tested up to 1 week	Capacitance	a = 31.5 b = 31	7
Glass/ PET/ PDMS/ Paper	Au nanonetwork	via liquid-liquid interface	87% (400-1000 nm)	YES	YES	Tested and stable up to 500 °C	tested and stable for more than a year	Current	a = 1.1 b = 1.3 (normal breathing)	Present study

References:

1. Y. Zhang, H. Ma, S. Wu, H. Yu, L. Wu, W. Li, J.-L. Sun, H. Wang and H. Fang, *Sens. Actuators Rep.*, 2022, **4**, 100092.
2. P. Songkeaw, K. Onlaor, T. Thiwawong and B. Tunhoo, *J. Mater. Sci: Mater. Electron*, 2020, **31**, 12206–12215.
3. Y. Wang, L. Zhang, J. Zhou and A. Lu, *ACS Appl. Mater. Interfaces*, 2020, **12**, 7631–7638.
4. H. Guo, C. Lan, Z. Zhou, P. Sun, D. Wei and C. Li, *Nanoscale*, 2017, **9**, 6246–6253.
5. J. Wu, Y. Chen, W. Shen, Y. Wu and J.-P. Corriou, *Ceram. Int.*, 2023, **49**, 2204–2214.
6. P.-G. Su, J.-Y. Tseng, Y.-C. Huang, H.-H. Pan and P.-C. Li, *Sens. Actuators B Chem.*, 2009, **137**, 496–500.
7. J. R. McGhee, J. S. Sagu, D. J. Southee and K. G. U. Wijayantha, *IEEE Sensors J.*, 2018, **18**, 7358–7364